Persistent quasiplanar nematic texture: Its properties and topological defects

Pawel Pieranski
Laboratoire de Physique des Solides, Université Paris-Sud, Bât. 510, 91405 Orsay, France

Maria Helena Godinho
i3N/CENIMAT, Department of Materials Science, Faculty of Science and Technology, Universidade NOVA de Lisboa, Campus de Caparica, 2829-516 Caparica, Portugal

Simon Čopar
Faculty of Mathematics and Physics, University of Ljubljana, Jadranska 19, 1000 Ljubljana, Slovenia
(Received 9 August 2016; revised manuscript received 4 October 2016; published 26 October 2016)

In the so-called quasiplanar texture of a nematic layer confined between parallel plates with homeotropic anchoring conditions, the director field rotates by π between limit surfaces so that field lines have the shape of a dowsing Y-shaped wooden tool. The orientation of the director field at midheight of the layer is arbitrary for symmetry reasons and is thus very sensitive to perturbations. We point out that contrary to accepted ideas the quasiplanar texture can be preserved infinitely in spite of its metastability with respect to the homogeneous homeotropic texture. We propose to call such a long-lived version of the quasiplanar texture *the dowser texture*. We demonstrate both experimentally and theoretically that in samples of variable thickness, the director field is sensitive to the gradient of the sample thickness through a linear coupling term. As a result, it has a tendency to follow the direction of the thickness gradient. Because of its sensitivity to perturbations we propose to call the midplane director field *the dowser field* and its tendency to follow the thickness gradient *cuneitropism*. Under effect of the gradient field, the dowser field obeys the sine-Gordon equation and exhibits domain walls that correspond to the well-known solitonic solutions of the sine-Gordon model.

DOI: 10.1103/PhysRevE.94.042706

I. INTRODUCTION

In many physical systems, including liquid crystals, lower-dimensional models are helpful for understanding the underlying phenomena but they usually also exhibit properties that are radically different from the full three-dimensional system. While these simplified models are theoretical exercises, approximate physical realizations can be constructed by geometrical restriction to a thin sample. Such experiments are invaluable for verifying theoretical results in the laboratory and are good hands-on educational tools.

In nematics, the two-dimensional model is especially enticing for its point defect topology, which differs from the three-dimensional counterpart [1]. The topological rules are directly reflected in the iconic two-dimensional visual pattern of the Schlieren texture [2] observed between crossed polarizers, which is practically a defining characteristic of nematic liquid crystals. Many specific quasi-two-dimensional nematic systems with varying degree of approximation to the true two-dimensional model have been studied—at free interfaces [3,4], in the form of shells [5] and umbilical systems [6], to name a few.

In this article, we present experiments on a long-lived metastable quasi-two-dimensional structure, dubbed the *dowser state*, represented by a two-dimensional vector field, dubbed the *dowser field*, which is sensitive to magnetic fields and is linearly coupled with sample thickness gradients. Experiments in the presence of thickness gradients obey the damped sine-Gordon equation, a well-known nonlinear model with solitonic solutions that parallels many physical systems [7,8]. We present preparation of the sample, discuss experiments that reveal characteristic properties of the dowser field, and discuss the parallel between the experiment and a theoretical model.

II. THE DOWSER TEXTURE

A. Production of the dowser texture

During recent experiments with disclination loops on Nylon fibers immersed in homogeneous homeotropic nematic samples (5CB) [9], we have observed that the homeotropic texture becomes unstable when the cell thickness is increased above a certain critical value h_{crit} depending on the radius of the sample.

This phenomenon has been studied in more details by means of a new setup (see Figs. 1 and 2), in which the nematic layer is contained between a glass plate and a plane-convex lens. There are no spacers maintaining the distance h between the lens and the glass slide, which have their own supports so that the lateral surface of the nematic sample (meniscus) is free. Minimization of the area of the free surface leads to the circular shape of radius R of the nematic layer and to its centering at the point O of the minimal thickness h_0.

At the 5CB/air interface the anchoring is homeotropic, too (see Fig. 2). As a result, the homeotropic texture of the sample is surrounded by the so-called quasiplanar texture [10–12], which matches the boundary conditions both at the meniscus and at the glass surfaces. In this quasiplanar texture the director rotates by π between the glass surfaces. Therefore, for topological reasons, the homeotropic and quasiplanar textures are separated by a disclination [13,14], which we call *peripheral* because it is located in the vicinity of the meniscus and encircles the sample.

Usually, in samples with a small aspect ratio h/R, this peripheral disclination stays in the vicinity of the meniscus so that the homeotropic texture is stable. However, when the aspect ratio is increased above a certain critical value, the peripheral disclination starts to shrink and finally collapses

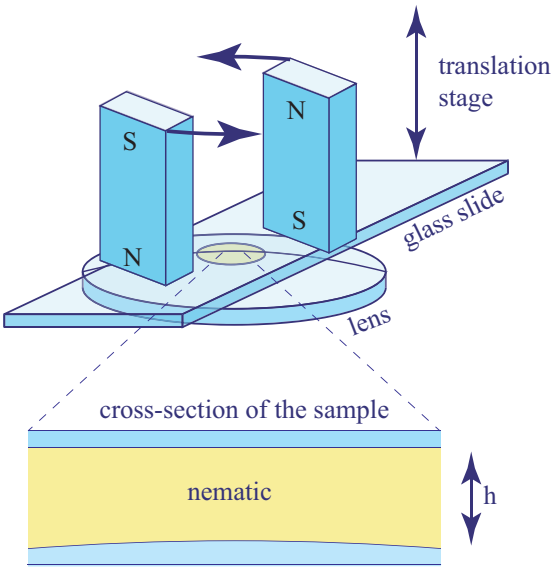

FIG. 1. Scheme of the setup.

into the *residual hedgehog* located in the center of the sample. This remarkable instability, observed for the first time by Gilli *et al.* [15], is illustrated by the series of six pictures in Fig. 3.

As a result of this homeotropic ⇒ quasiplanar transition occurring at the critical aspect ratio, the whole sample, except for the radial hedgehog, acquires the quasiplanar texture.

Experiments have shown that upon a subsequent reduction of the aspect ratio below the critical value the quasiplanar texture becomes metastable but the inverse quasiplanar ⇒ homeotropic transition does not take place unless the aspect ratio becomes lower than another, very small critical value.

With the aim to emphasize the robustness of the state in which the whole sample is filled with the quasiplanar texture we propose to call it *the dowser texture* for two reasons.

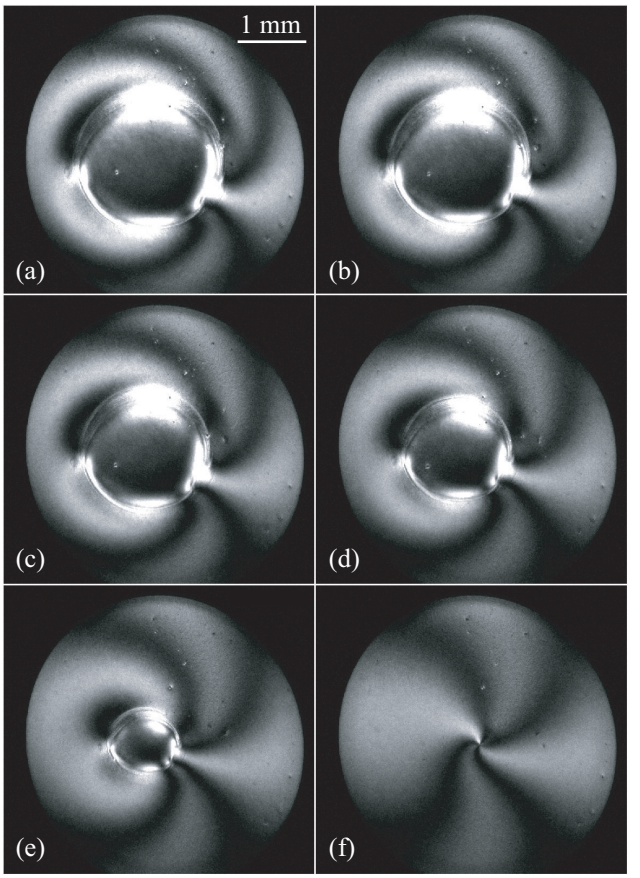

FIG. 3. Transition from the homeotropic into the dowser texture observed in a thick enough sample of 5CB: (a–e) shrinking of the peripheral disclination, (f) the dowser texture. It contains the residual hedgehog resulting from the collapse of the disclination.

First of all, the shape of the director field lines in the quasiplanar texture is similar to the dowser's Y-shaped wooden tool. In Fig. 2(e), the local direction of the dowser tool is

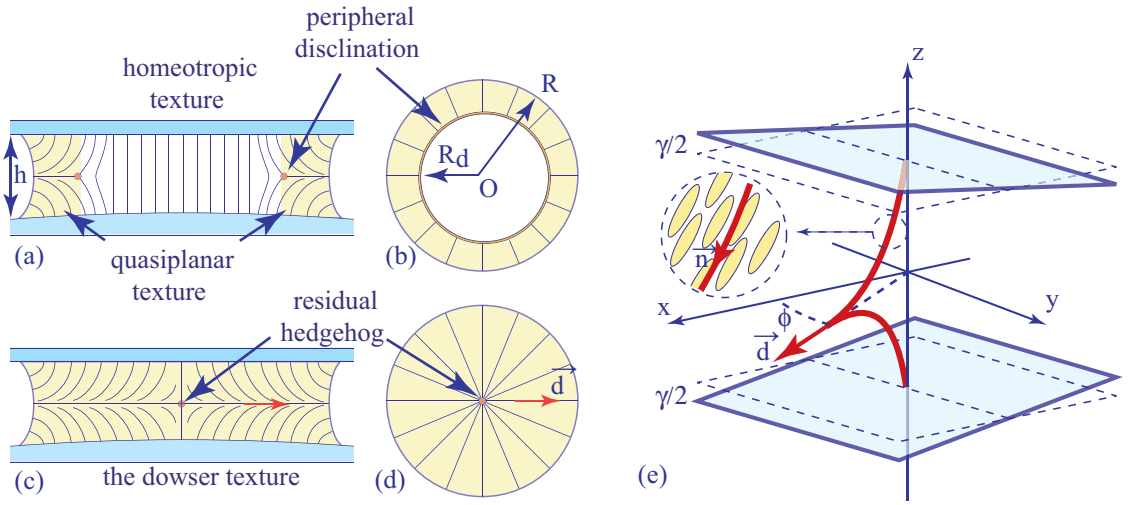

FIG. 2. Generation of the dowser texture: (a, b) coexistence of the homeotropic and quasiplanar textures separated by the peripheral disclination, (c, d) the dowser texture resulting from the collapse of the peripheral disclination. It contains the residual hyperbolic hedgehog, (e) perspective view of the dowser texture; the shape of the director field is reminiscent of the dowsing Y-shaped tool.

indicated by the vector **d**. When **d** varies in the xy plane, one can speak about *the dowser field* $\mathbf{d}(x,y)$.

The second reason is that the dowser field **d** is extremely sensitive to external fields. In particular, as we will point out both experimentally and theoretically, in samples of nonuniform thickness $h(x,y)$, such as the one in Fig. 2, the dowser field is sensitive to the thickness gradient $\mathbf{g} = \nabla h$. This phenomenon occurring in wedge-shaped samples is similar to the *geometrical anchoring* considered previously by de Gennes [16,17], Lavrentovich [4,19], and Link *et al.* [18]. We propose to call it *cuneitropism* from *cuneus* (wedge) and *tropism* (turning towards), referring to the tendency of the director to turn into the wedge direction.

B. Instability criterium of the homeotropic texture

The peripheral disclination of radius R_d [see Figs. 2(a) and 2(b)] is submitted to two competing forces: the centripetal Laplace force due to the tension T(h) (see f.ex. in Sec. 4.2.2. of Ref. [17]) of the peripheral disclination,

$$F_L = \frac{T(h)}{R_d} \approx \frac{E_c + K(\pi/4)\ln(h/r_c)}{R_d}, \tag{1}$$

where E_c is the energy of the disclination core and r_c its radius, and the opposing centrifuge force $F_{\rm dow}$ due to the difference in energies per unit area (see f.ex. in Sec. 3.1.3. of Ref. [17]) between the homeotropic and the dowser textures given by

$$F_{\rm dow} \approx \frac{\pi^2}{2}\frac{K}{h}. \tag{2}$$

Usually, during preparation of a homeotropic sample, $F_{\rm dow}(h) > F_L(R_d,h)$, so that the peripheral disclination increases its radius R_d and finally is pressed against the meniscus where it is stabilized by the short-ranged repulsive interaction with its virtual mirror image. In such a case the homogeneous homeotropic texture is stable, as wished in most of experiments.

However, when $F_{\rm dow}(h) < F_L(R_d,h)$, the radius R_d will decrease and the peripheral disclination will collapse in the center of the sample into the residual hyperbolic hedgehog as it has been shown in Fig. 3.

Quantitatively, the homogeneous homeotropic texture of maximal radius $R_d \approx R$ is unstable with respect to the *homeotropic* $\Rightarrow$ *dowser* transition when

$$R < R_{\rm crit} = h\frac{E_c/K + (\pi/4)\ln(h/r_c)}{\pi^2/2}. \tag{3}$$

Figure 4 illustrates the instability criterium for a sample of volume $V \approx \pi R^2 h = 10\,\text{mm}^3$ and typical values of the core energy $E_c/K \approx \pi/8$ and of the core radius $r_c \approx 500\,\text{Å}$ [14]. Consider a sample of radius $R = 3\,\text{mm}$, represented by the point H in this diagram. When the thickness h of this sample is increased, its radius evolves from H to D along the isochoric trajectory, drawn with the plain gray line, preserving the volume of the LC drop squeezed between the lens and the glass plate. Let h_u be the critical thickness corresponding to the crossing of the isochoric trajectory with the the line labeled "homeotropic → dowser transition" representing the stability criterium (3). After crossing this line, i.e., for $h > h_u$, the peripheral disclination will collapse and the homeotropic

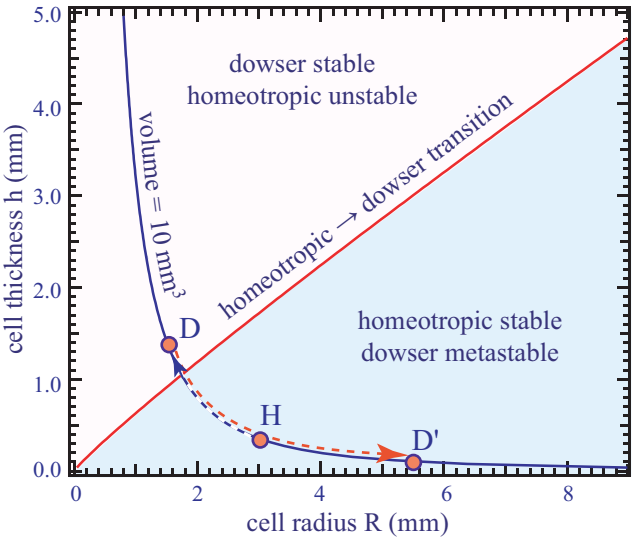

FIG. 4. Diagram of stability of the homeotropic and dowser textures. The dowser texture D is obtained from the homeotropic texture H on the isochoric trajectory HD by an adequate increase of the sample thickness. The dowser texture is preserved along the inverse DD′ trajectory in spite of its metastability.

texture will be transformed into the dowser texture. Let us note that in the interval $0 < R < 8\,\text{mm}$ the variation of the critical thickness h_u with R is approximately linear: $h_u \approx R/2$.

Our experiments unraveled a remarkable robustness of the dowser texture against the inverse *dowser* $\Rightarrow$ *homeotropic* transition. Indeed, upon a subsequent reduction of the sample thickness below h_u, for example along the dashed trajectory DD′, the dowser texture is preserved in spite of its metastability with respect to the homeotropic texture. This feature is obviously due to a prohibitive height of the barrier of transition from the hedgehog to a disclination loop state. In samples free of dust particles and other imperfections, the necessary disclination loop can still be generated from the residual hedgehog by reducing the sample thickness below a critical value calculated from Eq. (3), using the radius r_h of the hedgehog core. In practice, the dowser texture remains stable when h is larger than 0.1 μm, that is to say, in most experimental situations.

III. SENSITIVITY OF THE DOWSER FIELD, EXPERIMENTS

A. Winding of the dowser texture by a magnetic field

Thanks to the robustness of the dowser texture, we have tested its sensitivity to perturbations by magnetic fields. Among others, we performed experiments on winding the dowser field by means of a rotating magnetic field.

A typical experiment is illustrated here by Fig. 5, showing the result of application of a magnetic field followed by its rotation. This experiment is similar to the one made previously by Gilli *et al.* [15].

At the beginning of the experiment, the dowser field **d** has the radial structure shown in Fig. 5(a): it contains a $+2\pi$ disclination in its center (the hedgehog of the 3D director field **n**) and is orthogonal to the meniscus as expected. If ϕ is the

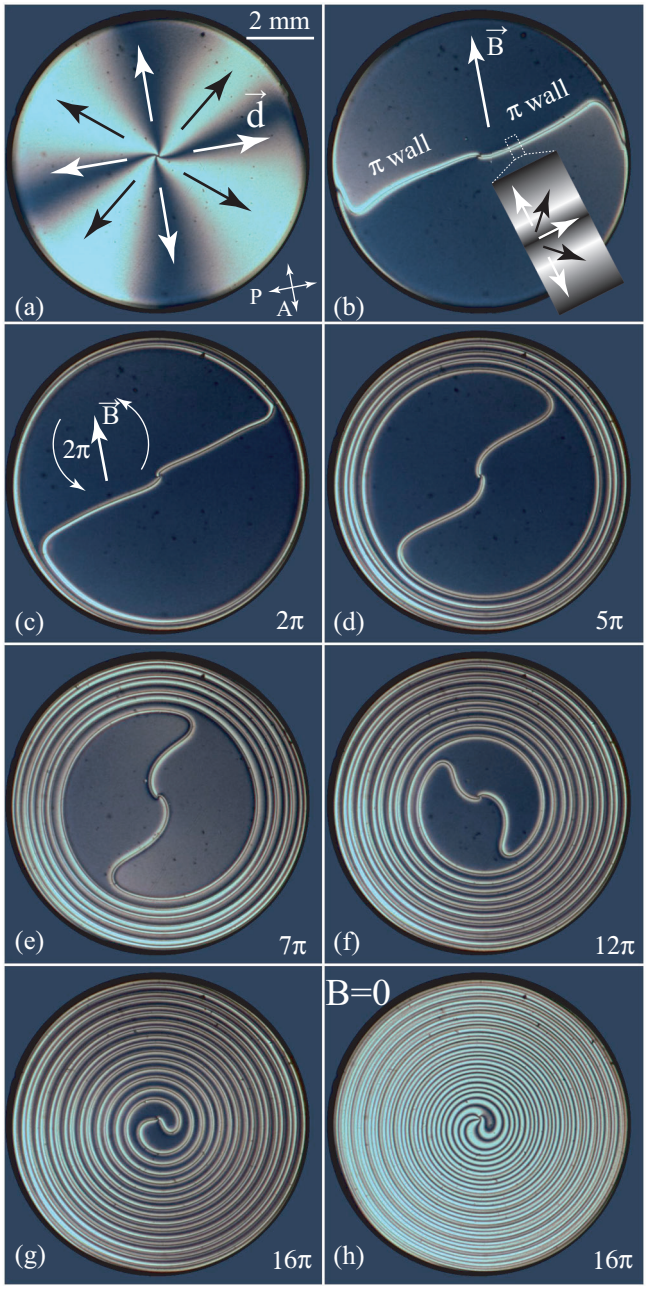

FIG. 5. Winding of the dowser texture by a rotating magnetic field: (a) initial radial dowser texture with a hedgehog in its center, (b) generation of two π walls by application of the magnetic field $\mathbf{B}$, (b–g) winding of the dowser texture by rotation of the magnetic field; the two π walls acquire spiral shapes, (h) the dowser texture after suppression of the magnetic field. The insert in picture b is a zoom on a small portion of the π wall; arrows represent the dowser field.

angle between $\mathbf{d}$ and the $\mathbf{x}$ axis then in polar coordinates (r,ψ) one has $\phi = \psi$.

After the application of the magnetic field $\mathbf{B}$ (by means of two magnets shown in Fig. 1) the dowser field $\mathbf{d}$ is aligned by it in parallel and antiparallel directions except for two almost straight π walls in which it rotates by π as shown in Fig. 5(b). The width $\xi_{\rm mag}$ of these π walls, resulting from the balance between elastic and magnetic torques, corresponds to the magnetic coherence length [16] given by expression

$$\xi_{\rm mag} \approx \sqrt{\frac{\mu_o K}{\chi_a}\frac{1}{B}}, \tag{4}$$

in which χ_a is the anisotropy of the magnetic susceptibility and K is the elastic constant in the single constant approximation.

Upon subsequent slow rotation of the magnetic field in the counterclockwise direction, the dowser texture is progressively wound. The winding process is illustrated in Fig. 5 by the series of five pictures (c–g) in which the two initially straight π walls are wound into spiral shapes. The last image in Fig. 5 shows the dowser texture after the removal of the magnetic field. In terms of the phase ϕ this dowser texture can be represented in polar coordinates as $\phi(r,\psi) = \psi + \phi_o f(r)$ with $f(0) = 1$ and $f(R) = 0$. By counting the number of black isogyres between $r = 0$ and $r = R$ in Fig. 5(h) one can infer that here $\phi_o = 8 \times 2\pi$. Moreover, the isogyres being almost equally spaced one can write $f(r) \approx 1 - r/R$.

B. Discovery of the cuneitropism: occurrence of 2π walls in a wound dowser field

In another experiment illustrated by the series of six pictures in Fig. 6 the initially radial dowser texture (a) has been wound by only four full turns of the magnetic field (b). Once the magnetic field was removed, the dowser field started its elastic relaxation and after 1.5 h [see Fig. 6(c)] the winding angle in the center was reduced by 2π to $\phi_o = 3 \times 2\pi$. In the next image taken after 7 h, the angle was $\phi_o = 2 \times 2\pi$. Then in Figs. 6(e) and 6(f) one has $\phi_o = 2\pi$ and $\phi_o = 0$.

When compared with results obtained in the experiment made with nematic layers of uniform thickness [20], the patterns of spiral-shaped isogyres in Figs. 6(c)–6(e) have a special unexpected feature: the isogyres are unevenly spaced along r. More precisely, they are assembled into groups of four isogyres which means that there are concentric 2π walls in the dowser field $\mathbf{d}(r,\psi)$.

We will show in Sec. IV that these concentric 2π walls are generated by a linear coupling between the dowser field $\mathbf{d}$ and the thickness gradient $\mathbf{g} = \nabla h$. The gap between the glass slide and the spherical lens depends on the radius as

$$h(r) = h_{\rm min} + R_l[1 - \sqrt{1 - (r/R_l)^2}], \tag{5}$$

and the gradient is

$$\mathbf{g} = \nabla h = \frac{r/R_l}{\sqrt{1-(r/R_l)^2}}\hat{\rho} = \gamma\hat{\rho}, \tag{6}$$

where R_l is the radius of curvature of the spherical lens and $\hat{\rho} = \mathbf{r}/|\mathbf{r}|$.

The four concentric 2π walls visible in Fig. 6 were generated by four full revolutions of the magnetic field. Other experiments have shown that the number, shapes, and topology of 2π walls generated by magnetic field depend on the angle $\phi_{\rm mag}$ of its rotation. As an example we show in Figs. 7(a)–7(d), 2π walls corresponding to $\phi_{\rm mag} = 125^\circ$ (a), 180° (b), 225° (c), and 360° (d).

In order to explain, for example, the triangular shapes of the two closed 2π walls in Fig. 7(b), we have to consider the detailed evolution of the dowser field represented

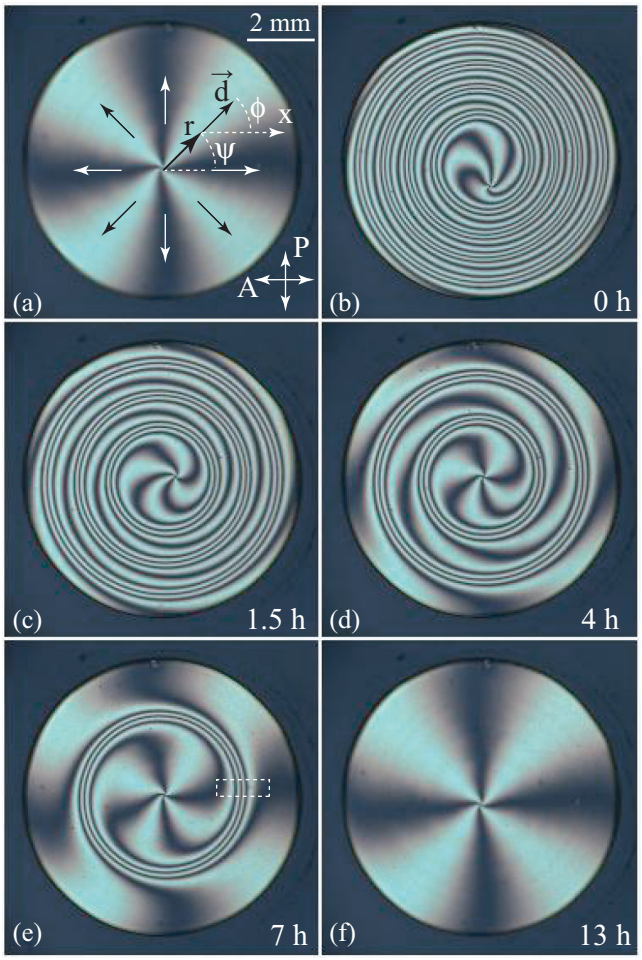

FIG. 6. Occurrence of 2π walls during unwinding of the dowser field. (a) Initial radial dowser field with a hedgehog in its center. (b) The dowser field wound in its center by $4 \times 2\pi$ by means of a rotating magnetic field. This picture was taken shortly after suppression of the magnetic field at the end of the winding process. (c–f) Continuation of the relaxation at $B = 0$. The winding angle in the center is, respectively, $3 \times 2\pi$ in (c), $2 \times 2\pi$ in (d), 2π in (e), and 0 in (f).

schematically in Figs. 7(e)–7(h). After the application of the magnetic field, the initially radial dowser field **d** [see Fig. 7(e)] rotates in clockwise or counterclockwise directions until it becomes parallel or antiparallel to **B**. As a result, two π walls orthogonal to the field are created [Fig. 7(f)]. Subsequently, the dowser field **d** follows the rotation of the magnetic field **B** by π in the counterclockwise direction. After the suppression of the magnetic field, the linear coupling of the dowser field **d** with the radial thickness gradient field **g** will exert torques on the dowser field. In sectors NE and SW [defined in Fig. 7(f)] the dowser field **d** will rotate back in clockwise direction until it becomes parallel to **g**. In sectors NW and SE **d** will continue its anticlockwise rotation until it becomes parallel to **g**. In conclusion, after relaxation, the NO and SE sectors must be separated, for topological reasons, by 2π walls from the rest of the sample.

In the case $\phi_{\text{mag}} = 2\pi$ [Fig. 7(d)] one circular 2π wall is generated. Observation of this wall during several hours unveils its slow collapse illustrated by the series of four pictures, Figs. 8(a)–8(d) and by the spatiotemporal cross-section shown in Fig. 8(e). Let us stress that while the wall's radius R_w decreases to zero its width ξ decreases too. The discussion of this behavior will be resumed in Sec. IV C.

C. Second evidence of cuneitropism: A straight radial 2π wall

The second evidence for the existence of the linear coupling between the dowser field **d** and the thickness gradient **g** has been provided by the pattern of isogyres modified by the shift of the residual hedgehog toward the edge of the nematic droplet.

In the case when the hedgehog is located in the center of the sample [see Fig. 9(a)], the pattern of isogyres has the aspect of the maltese cross, which means that the dowser field **d** has the radial structure identical with the one in Fig. 6(a).

Let us note that in Figs. 9(a) and 9(b) which have been obtained with monochromatic light, beside isogyres, concentric black interference fringes are well visible too. These are isochromes—lines of equal phase shift $\Delta\phi = 2\pi\,\Delta n h/\lambda = N2\pi$ between the ordinary and extraordinary rays. For $\Delta n = \text{const}$, these isochromes are also lines of equal thickness h. The thickness gradient **g** has, therefore, as expected from the sphere and plane geometry, the radial structure and its center coincides with the center of the dowser field. In conclusion, one has **d**||**g**.

In the sphere and plane geometry, the dowser texture with the residual hedgehog in the center corresponds to the minimum of energy. In practice, a long relaxation process is necessary to reach this ground state. Most of the time, after manipulations of the sample (winding by the magnetic field followed by changes in the sample thickness) the dowser texture contains many hedgehog whose total number is always odd for topological reasons. During the subsequent evolution toward the energy minimum, annihilation of hedgehogs by pairs occurs. In general, at the end of the annihilation process the position of the residual hedgehog in the sample is out of the center. In Fig. 9(b), the hedgehog H is shifted toward the edge of the sample. As a result, the pattern of the isogyres connected to the hedgehog is modified by the interaction with the gradient field: the isogyres are first bundled together into the 2π wall going from the hedgehog to the sample center O where they separate and take the radial directions forced by the gradient field.

The detailed structure of this straight 2π wall is resolved in the close-up shown in Fig. 9(c).

D. Third evidence of cuneitropism: relaxation

The third evidence of the $\mathbf{g} \cdot \mathbf{d}$ coupling comes from observations of its contribution to relaxation. A typical experiment of this kind is illustrated by the series of six images in Fig. 10. The first image (a) shows the equilibrium state of the dowser field with the hedgehog in the center submitted to the action of the horizontal magnetic field **B**. As already mentioned before, the magnetic field **B** imposes orientations of the dowser field **d** parallel and antiparallel to **B** and leads to formation of two π walls. When the magnetic field is suppressed, the dowser field relaxes into its initial equilibrium radial configuration shown

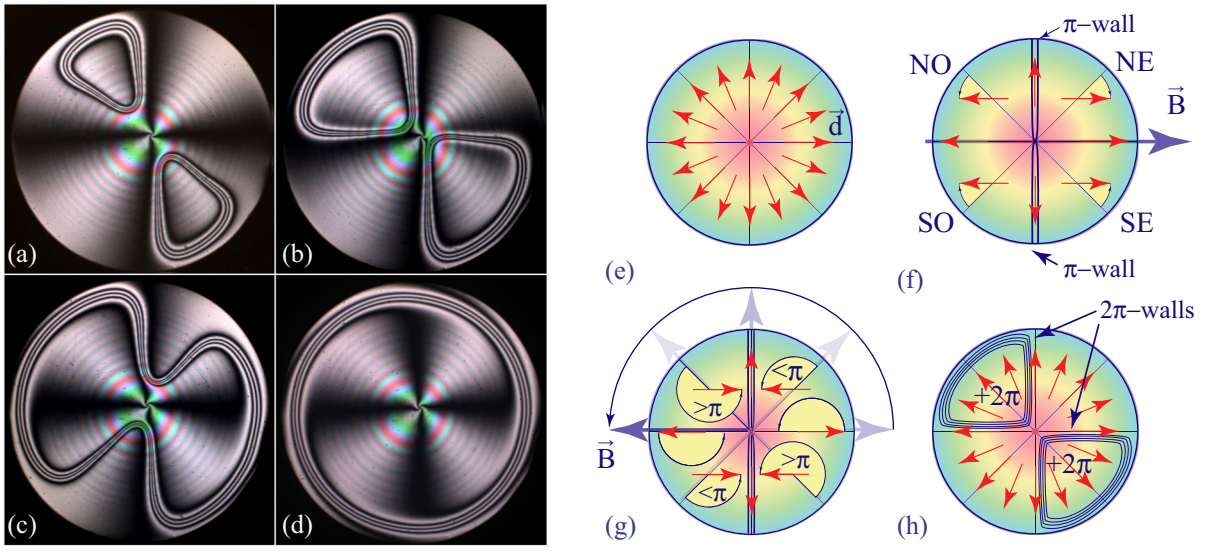

FIG. 7. 2π walls generated by rotation of the magnetic field by the angle $\phi_{\mathrm{mag}} = 125^\circ$ (a), 180° (b), 225° (c), and 360° (d). (e–h) Explanation of the generation of the two 2π walls by the $\phi_{\mathrm{mag}} = 180^\circ$ rotation of the magnetic field shown in (b): (e) initial radial dowser field with a hedgehog in its center, (f) application of the magnetic field, (g) rotation of the magnetic field by 180°, (h) formation of the two 2π walls after suppression of the field.

in Fig. 10(f), in which **d** is parallel to **g**. Let us stress that the characteristic relaxation time is of the order of six minutes.

As we will see later in Sec. IV, this relaxation is driven by two torques: the elastic one [the first term in Eq. (13)], which would exist in a sample of uniform thickness and the cuneitropic one [the second term in Eq. (13)], resulting from the coupling with the thickness gradient. If the elastic torque was acting alone, in the sample having the size of a few millimeters in diameter the relaxation time would be of the order of few hours instead of 6 min. We can therefore conclude that only the $\mathbf{g} \cdot \mathbf{d}$ coupling can drive such a rapid relaxation.

IV. CUNEITROPISM OF THE DOWSER FIELD, THEORETICAL MODEL AND CALCULATIONS

A. Coupling between the dowser field and the thickness gradient

To understand the coupling between the dowser field and the thickness gradient, let us consider first the dowser texture in a sample of uniform thickness, as shown in Fig. 11(a). Here, director field rotates by $\alpha = \pi$ between the limit plates separated by the distance h. The energy of distortion per unit area in the approximation of the isotropic elasticity is

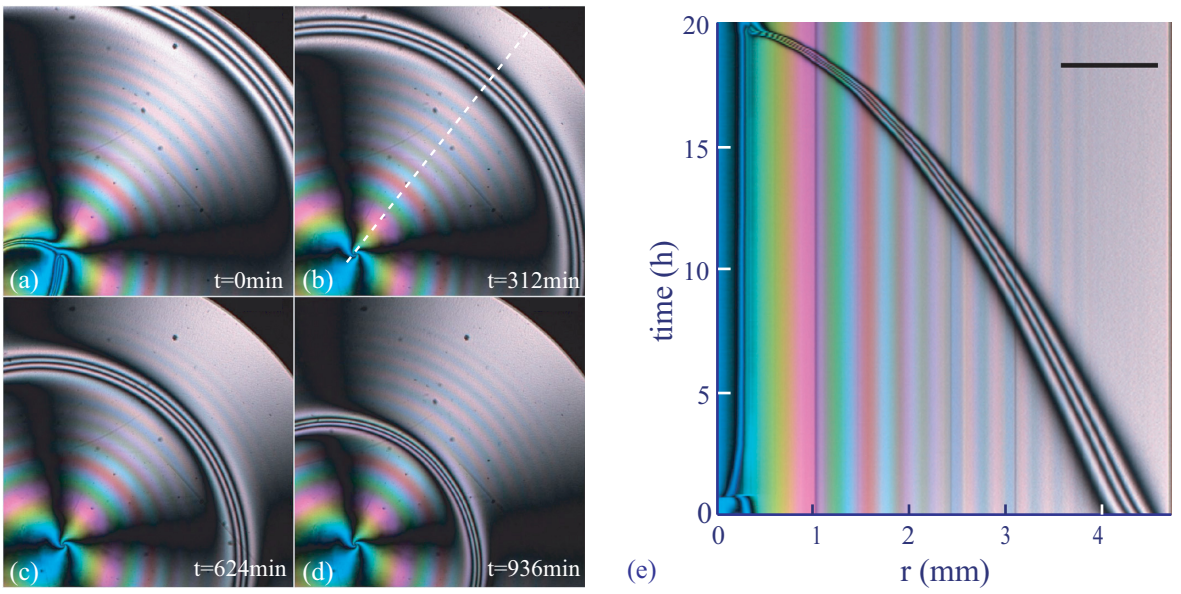

FIG. 8. Collapse of a circular 2π wall: (a–d) four pictures selected from a video, (e) spatiotemporal cross-section of the video taken along the dotted line defined in (b).

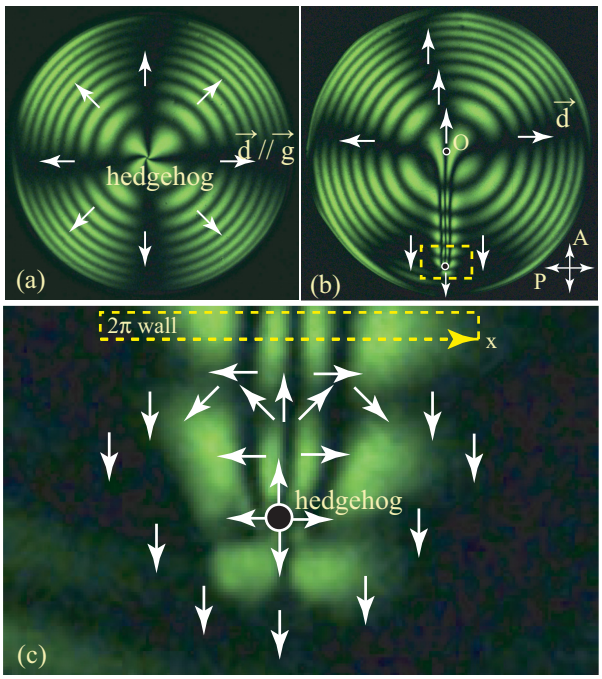

FIG. 9. Generation of a straight radial 2π wall: (a) pattern of isogyres and isochromes of a sample with the residual hedgehog in its center, (b) pattern of isogyres modified by the shift of the hedgehog toward the sample edge, (c) close-up of the 2π wall connected to the hedgehog.

given by

$$F_{\text{dow}} = \int_0^h \frac{K}{2}\left(\frac{\alpha}{h}\right)^2 dz = \alpha^2 \frac{K}{2h}. \tag{7}$$

For symmetry reasons, this expression does not depend on the azimuthal orientation ϕ of the dowser field $\mathbf{d}$ when the thickness is uniform.

When the upper plate is tilted by an angle γ [Fig. 11(b)], the director rotates by the angle $\alpha = \pi - \gamma\cos\phi$, where we recall $\gamma\cos\phi = \mathbf{g}\cdot\mathbf{d}$. The energy of the dowser state becomes

$$F_{\text{dow}} = (\pi - \gamma\cos\phi)^2\frac{K}{2h} \approx \pi^2\frac{K}{2h} - \frac{\pi K}{h}\mathbf{g}\cdot\mathbf{d}. \tag{8}$$

Thus, the dowser field $\mathbf{d}$ linearly couples with the thickness gradient $\mathbf{g}$ and tends to align along the gradient.

B. 2π wall as a soliton

In a general case when the dowser field is not uniform in the xy plane, the coupling term is in competition with the elastic energy per unit area, which can be written as $\frac{1}{2}K_{\text{eff}}h(\nabla\phi)^2$ where K_{eff} describes the joint contributions of different elastic modes to the deformation free energy. Therefore, in equilibrium, the dowser field has to minimize the functional

$$F_{\text{tot}} = \int\left[\frac{K_{\text{eff}}h}{2}(\nabla\phi)^2 - \frac{\pi K}{h}\mathbf{g}\cdot\mathbf{d}\right]dxdy. \tag{9}$$

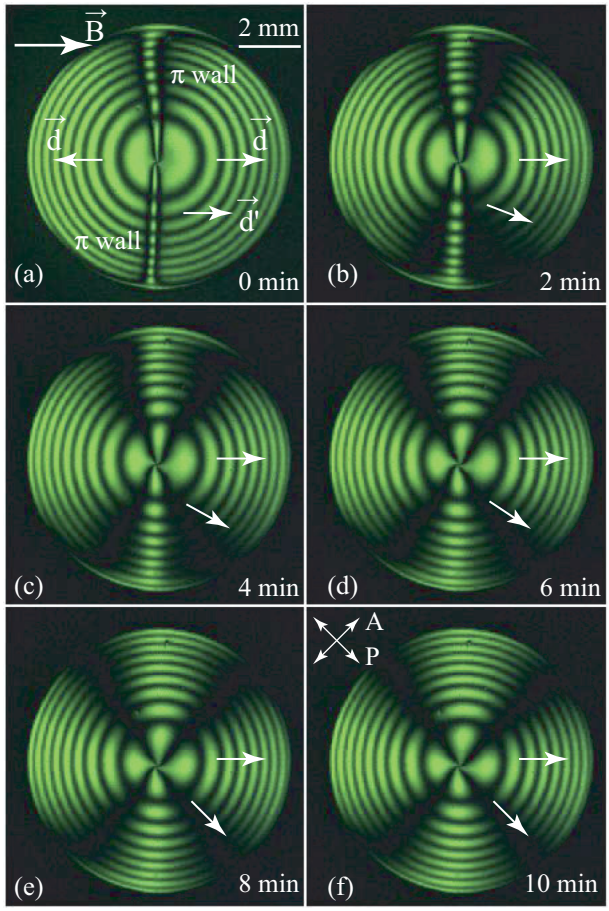

FIG. 10. Relaxation of the dowser field: (a) two π walls in the dowser field aligned by the magnetic field $\mathbf{B}$, (b–f) relaxation toward the radial configuration driven by the -$\mathbf{g}\cdot\mathbf{d}$ coupling.

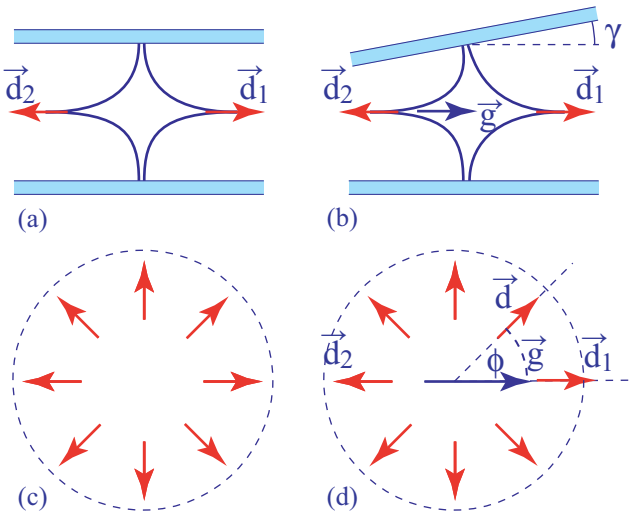

FIG. 11. Explanation of the coupling between the dowser field $\mathbf{d}$ and the thickness gradient $\mathbf{g}$: (a–c) between parallel plates, the energy of the dowser field does not depend on its orientation, (b–d) in a wedge, the energy depends on the angle ϕ between the dowser field $\mathbf{d}$ and the thickness gradient $\mathbf{g}$. For example, the distortion energy of $\mathbf{d}_1$ is lower than that of $\mathbf{d}_2$.

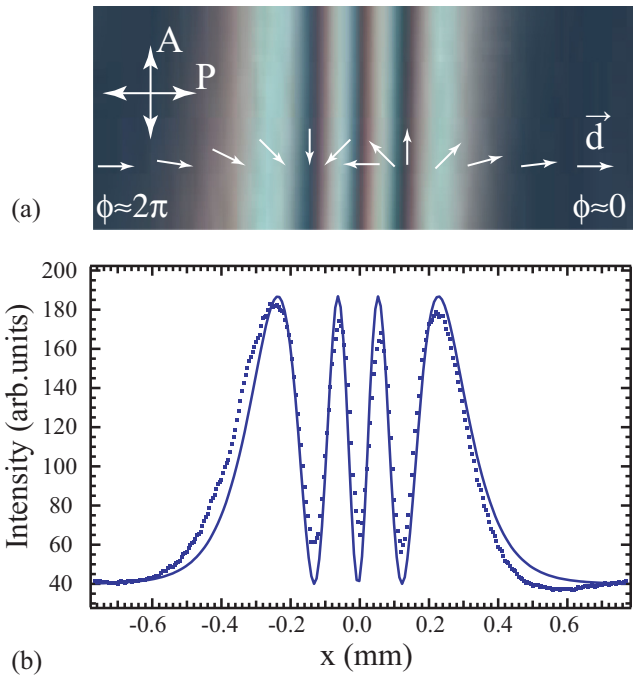

FIG. 12. Analysis of the isogyres pattern in the 2π wall: (a) enlargement of the rectangle from Fig. 6(e); (b) dots: data extracted from a, line: fit to the equation (14) with ϕ given by Eq. (12).

In the simplest case of flat glass plates forming a wedge of angle γ [Fig. 11(b)], the gradient vector $\mathbf{g}$ is constant and variation of the functional [Eq. (9)] yields the equation

$$\nabla^2\phi - \frac{1}{\xi^2}\sin\phi = 0, \tag{10}$$

which in one dimension reduces to the pendulum equation. The parameter

$$\xi = h_0\sqrt{\frac{K_{\text{eff}}}{K}\frac{1}{\pi\gamma}} \tag{11}$$

is the characteristic width of the 2π wall. The solution, compatible with the boundary conditions $\phi(\pm\infty)$ of the 2π wall correspond to the critical solution (also known as the Abrarov solution) of the pendulum equation in the form

$$\phi = 4\arctan e^{\pm x/\xi}, \tag{12}$$

which gives the theoretical prediction of the director profile of the wall.

Equation (10) is the sine-Gordon equation, which is a textbook model that exhibits solitonic solutions with the profile described by Eq. (12) [7,8].

Out of this equilibrium state, there is viscous relaxation of the director, and Eq. (10) generalizes to the damped version of the sine-Gordon equation [21,22]:

$$\nabla^2\phi - \frac{1}{\xi^2}\sin\phi = \frac{1}{D_{\text{dow}}}\frac{\partial\phi}{\partial t}. \tag{13}$$

Here, D_{dow} is the diffusivity of the dowser field. Due to very slow relaxation, the effects of flow can be neglected. This equation is a textbook model that exhibit solitonic solutions with the profile given by Eq. (12) [7,8] and describe many other 2D physical systems that can be represented as a xy model in external field [23,24].

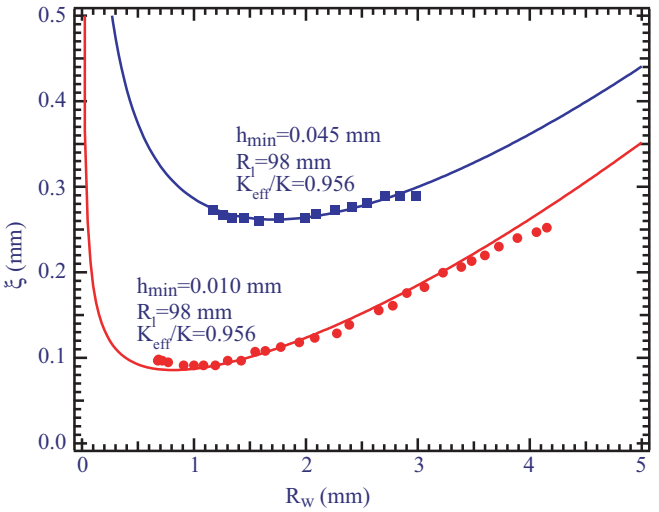

FIG. 13. Dependence of the 2π wall's width on its radius.

C. The circular 2π wall in the dowser field

Figure 12(b) shows the intensity profile,

$$I \propto \sin^2(2\phi), \tag{14}$$

corresponding to the director profile in the 1D case, fitted to the experimental data in Fig. 12(a) extracted from Fig. 6(e). Even though in the sphere and plane geometry of the cell the thickness γ varies slightly across the wall, the fit is very good and delivers the 2π-wall thickness parameter $\xi \approx 0.143$ mm, which can be compared to the theoretical prediction given by Eq. (11).

For this purpose, the width ξ has been measured during the slow collapse of the wall (such as the one in Fig. 8). Results obtained with two samples of different thicknesses are plotted using circular and square markers versus the wall's radius R_w in Fig. 13. The theoretical fits drawn with continuous lines have been made using Eq. (11), in which the thickness h_0 has been replaced by the local thickness from Eq. (5) and the slope γ is given by Eq. (6).

The fitting parameters were the ratio of elastic constants K_{eff}/K, the curvature radius of the lens R_l, and the minimal distance h_{min} between the lens and the glass plate. Their values corresponding to the best fits are indicated in Fig. 13.

Let us emphasize that the local width of the 2π wall given by Eq. (11) decreases first during the collapse but when the wall radius R_w tends to 0 it diverges because the slope γ vanishes in the center of the plane and sphere gap.

D. Effects of the elastic anisotropy

A more detailed analysis of the structure of 2π walls should take into account the elastic anisotropy of the dowser field whose distortion energy density (per unit area), expressed in terms of the two possible scalar invariants $\vec{\nabla}\cdot\mathbf{d}$ and

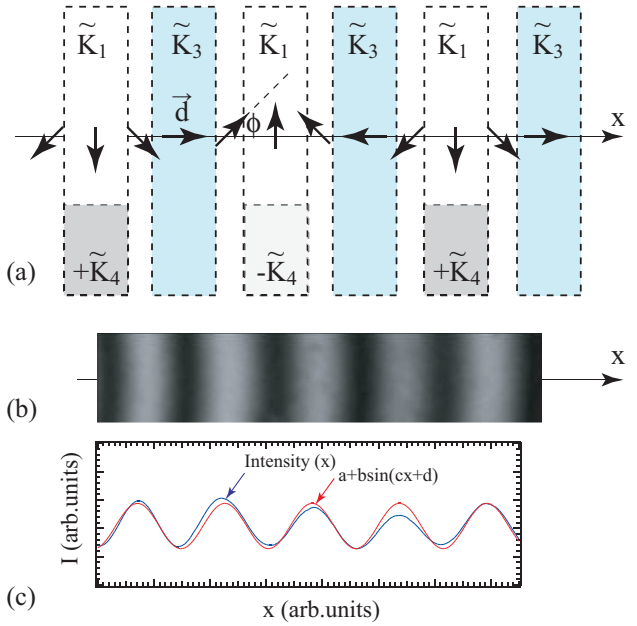

FIG. 14. Effects of anisotropic elasticity in wound dowser field. (a) Identification of the splay, bend, and saddle-splay deformations of the dowser field. (b) interference pattern of a wound dowser field observed in a polarizing microscope. (c) Line labeled "Intensity(x)": measured intensity; line labeled "a+bsin(cx+d)": fit to this sin function.

$(\mathbf{d} \times (\vec{\nabla} \times \mathbf{d}))^2$, can be written as

$$f = h\left[\frac{1}{2}\widetilde{K}_1(\vec{\nabla}\cdot\mathbf{d})^2 + \frac{1}{2}\widetilde{K}_3(\mathbf{d}\times(\vec{\nabla}\times\mathbf{d}))^2 + \frac{\widetilde{K}_4}{h}\vec{\nabla}\cdot\mathbf{d}\right]. \tag{15}$$

The first two terms correspond, respectively, to splay and bend distortions of the dowser field and the effective elastic constants $\widetilde{K}_1$ and $\widetilde{K}_3$ depend on the detailed 3D structures of the director field. Due to the vector character of the dowser field $\mathbf{d}$, this expression needs not to be invariant with respect to the sign reversal $\mathbf{d} \to -\mathbf{d}$ so that the last term linear in $\vec{\nabla}\cdot\mathbf{d}$ is allowed. It corresponds to the "saddle-splay" distortion of the director field involving second order derivatives of the director field such as $\partial_z\partial_x$ and $\partial_z\partial_y$. In Eq. (15), the derivative with respect to z is implicit and results in the 1/h dependence of its elastic coefficient.

Let us suppose that the orientation ϕ of a wound dowser field varies only with x as shown in Fig. 14(a). In such a case one obtains

$$f = h\left\{\frac{1}{2}[\widetilde{K}_1\sin^2(\phi) + \widetilde{K}_3\cos^2(\phi)]\left(\frac{d\phi}{dx}\right)^2 - \frac{\widetilde{K}_4}{h}\sin(\phi)\frac{d\phi}{dx}\right\}. \tag{16}$$

In the approximation used in Sec. III C with $\widetilde{K}_1 = \widetilde{K}_3$ and $\widetilde{K}_4 = 0$, minimization of the functional $\int f dx$ would lead to a linear solution $\phi(x) = ax$; in experiments, isogyres in the interference patterns would be equally spaced.

If, on the other hand, $\widetilde{K}_3$ was much larger than $\widetilde{K}_1$ and $\widetilde{K}_4$ was still zero, the function $\phi(x)$ would be more complex: in bands with the bend distorsion variation of ϕ with x would be slower then in bands with the splay distortion. As a result, the width of isogyres would vary periodically with x: large and narrow fringes would alternate. Finally, if the saddle-splay term was important, each fourth fringe would have a different width than the three other.

Let us compare now these theoretical predictions with a typical interference pattern obtained in an experiment made with a thick sample and shown in Fig. 14(b). The corresponding variation of the intensity $I(x)$ is plotted with the line labeled "Intensity(x)" in Fig. 14(c). The second plot labeled "a+bsin(cx+d)" in the same diagram is a fit to the linear variation of ϕ with x obtained in the isotropic case. We can conclude that the isotropic approximation used in Sec. III C is justified in practice *a posteriori*.

V. CONCLUSIONS

The breakthrough of the present work consists in showing that contrary to the accepted ideas the quasiplanar texture can be infinitely preserved in spite of its metastability with respect to the homogeneous homeotropic state.

Such a long-lived quasiplanar texture that we call the dowser state is a broken symmetry state that is characterized by the 2D dowser field describing the local xy orientation of the midplane director. In the sample of a uniform thickness, all the directions are degenerate, which makes the dowser field very sensitive to perturbations, such as external fields and sample inhomogeneities.

Experiments with the dowser state described here have unraveled the cuneitropism of the dowser field, or, in other words, its tendency to align in the direction of the thickness gradient, similar to the mechanism of geometric anchoring discovered by Lavrentovich [4]. This phenomenon parallels with many other two-dimensional systems with linear coupling to an external field which obey the sine-Gordon equation, such as the classical xy spin systems, ferroelectrics, and charge-density waves [7,8]. As such, the dowser state is a table-top realization of the damped sine-Gordon model, where the solitonic solutions appear as 2π walls and can be easily observed under the microscope. In addition, the dowser field couples both to the thickness gradient field and to the external magnetic field, which allows for many interesting experiments with the sine-Gordon model which would be more difficult to perform on the scale of solid state systems.

ACKNOWLEDGMENTS

This work benefited from collaboration with R. Veronneau and R. Taktak. We thank I. Dozov who offered us the nematic 5CB used in this study. The authors also thank V. Klein, S. Saranga, J. Sanchez, J.-L. Signoret, M. Bottineau, J. Vieira, and A. Lecchi for technical help. This work is funded by FEDER funds through the COMPETE 2020 Program and National Funds through FCT–Portuguese Foundation for Science and Technology under the Projects Numbers POCI-01-0145-FEDER-007688 (Reference UID/CTM/50025) and PTDC/CTM-BIO/6178/2014. S.Č. acknowledges support by Slovenian Research Agency (ARRS) under Grants No. P1-0099 and No. Z1-6725.

[1] N. Mermin, The topological theory of defects in ordered media, Rev. Mod. Phys. **51**, 591 (1979).
[2] A. Saupe, Disclinations and properties of the directorfield in nematic and cholesteric liquid crystals, Mol. Cryst. Liq. Cryst. **21**, 211 (1973).
[3] R. B. Meyer, Point disclinations at a nematic-lsotropic liquid interface, Mol. Cryst. Liq. Cryst. **16**, 355 (1972).
[4] O. D. Lavrentovich, Geometrical anchoring at an inclined surface of a liquid crystal, Phys. Rev. A **46**, R722 (1992).
[5] V. Vitelli and D. Nelson, Nematic textures in spherical shells, Phys. Rev. E **74**, 021711 (2006).
[6] I. Dierking, O. Marshall, J. Wright, and N. Bulleid, Annihilation dynamics of umbilical defects in nematic liquid crystals under applied electric fields, Phys. Rev. E **71**, 061709 (2005).
[7] *The Sine-Gordon Model and its Applications: From Pendula and Josephson Junctions to Gravity and High-Energy Physics*, edited by J. Cuevas-Maraver, P. G. Kevrekidis, and F. Williams (Springer International Publishing, Berlin, 2014).
[8] A. R. Bishop, Solitons in condensed matter physics, Phys. Scr. **20**, 409 (1979).
[9] S. Čopar, D. Seč, L. E. Aguirre, P. L. Almeida, M. Dazza, M. Ravnik, M. H. Godinho, P. Pieranski, and S. Žumer, Sensing and tuning microfiber chirality with nematic chirogyral effect, Phys. Rev. E **93**, 032703 (2016).
[10] V. S. U. Fazio, L. Komitov, and S. T. Lagerwall, Alignment and alignment dynamics of nematic liquid crystals on Langmuir-Blodgett mono-layers, Liq. Cryst. **24**, 427 (1998).
[11] V. S. U. Fazio, and L. Komitov, Alignement transition in a nematic liquid crystal due to field-induced breaking of anchoring, Europhys. Lett. **46**, 38 (1999).
[12] V. S. U. Fazio, L. Komitov, C. Raduge, S. T. Lagerwall, and H. Motschmann, Influence of the flow on the anchoring of nematic liquid crystals on Langmuir-Blodgett monolayers studied by optical second-harmonic generation, Eur. Phys. J. E **5**, 309 (2001).
[13] J. Ignés-Mullol, J. Baudry, L. Lejcek, and P. Oswald, Formation of disclination lines near a free nematic interface, Phys. Rev. E **59**, 568 (1999).
[14] P. Oswald and P. Pieranski, *Nematic and Cholesteric Liquid Crystals* (Taylor & Francis, London, 2005), Chap. B. IV.
[15] J. M. Gilli, S. Thiberge, A. Vierheilig, and F. Fried, Inversion walls in homeotropic nematic and cholesteric layers, Liq. Cryst. **23**, 619 (1997).
[16] P.-G. de Gennes, Structures en domaines dans un nématique sous champ magnétique, Solid State Commun. **8**, 213 (1970).
[17] P.-G. de Gennes and J. Prost, in *The Physics of Liquid Crystals* (Clarendon Press, Oxford, 1993), pp. 174–175.
[18] D. R. Link, M. Nakata, Y. Takanishi, K. Ishikawa, and H. Takezoe, Patterns in Hybrid Nematic Liquid-Crystal Films, Phys. Rev. Lett. **87**, 195507 (2001).
[19] O. D. Lavrentovich and V. M. Pergamenshchik, Patterns in thin liquid crystal films and the divergence ("surfacelike") elasticity, Int. J. Mod. Phys. B **09**, 2389 (1995).
[20] P. Pieranski, Generation of umbilics by Poiseuille flows, Eur. Phys. J. E **37**, 24 (2014).
[21] J. Rubinstein, Sine-Gordon equation, J. Math. Phys. **11**, 258 (1970).
[22] K. Djidjeli, W. G. Price, and E. H. Twizell, Numerical solutions of a damped Sine-Gordon equation in two space variables, J. Eng. Math. **29**, 347 (1995).
[23] H.-J. Mikeska and M. Steiner, Solitary excitations in one-dimensional magnets, Adv. Phys. **40**, 191 (1991).
[24] M. E. Gouveat, F. G. Mertens, A. R. Bishop, and G. M. Wysin, The classical two-dimensional XY model with in-plane magnetic field, J. Phys.: Condens. Matter **2**, 1853 (1990).